Structure and growth of crystalline superlattices: From monolayer to superlattice

E. Bauer* and Jan H. van der Merwe
Department of Physics, University of Pretoria, Pretoria 0001, Republic of South Africa
(Received 28 August 1985)

We discuss the physical phenomena fundamental to the understanding of the structure and growth of crystalline superlattices: (i) the growth mode as determined by surface energies, supersaturation, and lattice misfit; and (ii) the dependence of epitaxial orientation on lattice matching, atomic bonding, and film thickness, in the topical case of epitaxy at (111) fcc/(110) bcc interfaces. For uniformity monolayer-by-monolayer [Frank–van der Merwe (FM)] growth is desirable. This may be adversely affected by the formation of misfit dislocations. Continued FM growth may be achieved with alternate A and B layers at moderate supersaturation, provided that the surface energies γ_A and γ_B are compatible. The suggestion that it is possible otherwise at sufficiently high supersaturation is a misconception. The main epitaxial orientations in the present case—the Nishiyama-Wassermann (NW) and the Kurdjumov-Sachs (KS) orientations—have been previously predicted on the (energetically justified) basis of geometrical relationships alone. The predictive power of this model is demonstrated for hexagonal interfaces. Ideally, to predict the evolution of the structure and orientation of a growing (thickening) film atomic forces must be allowed for. We model these forces by means of crystallinity and harmonicity of film, and by a truncated–Fourier-series adsorbate-substrate interaction. Various forms of homogeneous and oscillatory film strains, affecting orientation and structure, are illustrated graphically. We conclude that a good guideline for superlattice formation is the following: (a) growth at moderate supersaturations of metal pairs with comparable γ's in the unique NW orientation ($0.8 \lesssim b/a \lesssim 1.0$, a and b are nearest-neighbor distances); or, possibly, (b) nucleation and growth along unidirectional steps.

I. INTRODUCTION

Artificial metallic superlattices have recently gained increasing interest due to their unusual physical properties.[1] While in semiconductor superlattices lattice matching is of paramount importance to ensure suitable electronic properties, no such restrictions occur for metallic superlattices. In fact, most of the metallic superlattices studied to date consist of components with different crystal structure (fcc/bcc metal pairs) and with differences in the atomic radii as large as 10% (Cu-Nb).[2] Although epitaxial monolayer and multilayer formation is observed for many metal/metal combinations,[3] only a few metal/metal combinations have yielded crystalline superlattices to date. This problem was recently addressed by Ramirez *et al.*[4] The present paper goes beyond the approximations made in that study and thus gives a much deeper insight into the processes which are of importance in the transition from a monolayer to a superlattice.

A superlattice consisting of the metals A and B is called *crystalline* if all A regions have the same crystallographic orientation as well as all B regions. A superlattice is called *layered* if in all A regions a certain crystallographic plane—usually the most densely packed plane—is parallel and if the same is true for all B regions.[4] Thus, in a layered superlattice azimuthal misorientation of the parallel planes are allowed, while the crystalline superlattice requires complete mutual epitaxy of the two metals. This paper is concerned only with crystalline superlattices, and in particular with superlattices consisting of stacking sequences of densely packed planes, i.e., (111) fcc, (0001) hcp, and (110) bcc planes. The relative orientation of the two components A and B is determined by the condition that the total system is in the state of minimum free energy under the geometrical constraint imposed by the requirement that the system should form a superlattice. The theoretical determination of this state, which involves locally strongly varying strains, is a formidable problem which can be solved only approximately.

This is done in the following section at various levels of sophistication for a monolayer. Section III is concerned with the transition from monolayer to multilayer and superlattice. In Sec. IV the question as to what extent the geometrical constraint of plane-parallel growth can be achieved is discussed. Section V compares theory and experiment for monolayers and multilayers which leads to realistic predictions of superlattice structure and growth (Sec. VI). The findings are summarized in Sec. VII.

II. THE STRUCTURE OF THE MONOLAYER

The simplest approximation is the assumption that both lattices A and B are rigid (rigid-lattice approximation). In this case the orientation relationship is essentially independent of the relative thickness of the component layers and the interactions within and between the layers. Only the geometries of the two lattices determine the minimum-energy configuration, provided physically reasonable interactions are used. Therefore, purely geometrical considerations allow already important orientation predictions. For (111) fcc/(111) fcc or (0001) hcp interfaces such considerations are discussed in Appendix

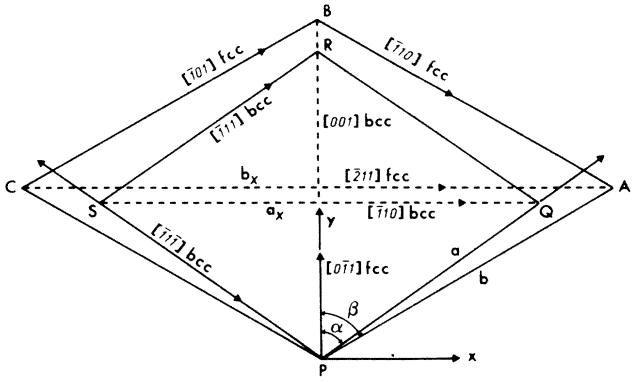

FIG. 1. Rhombic unit cells of a (111) fcc or (0001) hcp monolayer and a (110) bcc substrate, showing Cartesian axes, crystal directions, angles $\alpha=\arctan\sqrt{2}$ and $\beta=60°$, nearest-neighbor distances a and b, and diagonal lengths a_x and b_x.

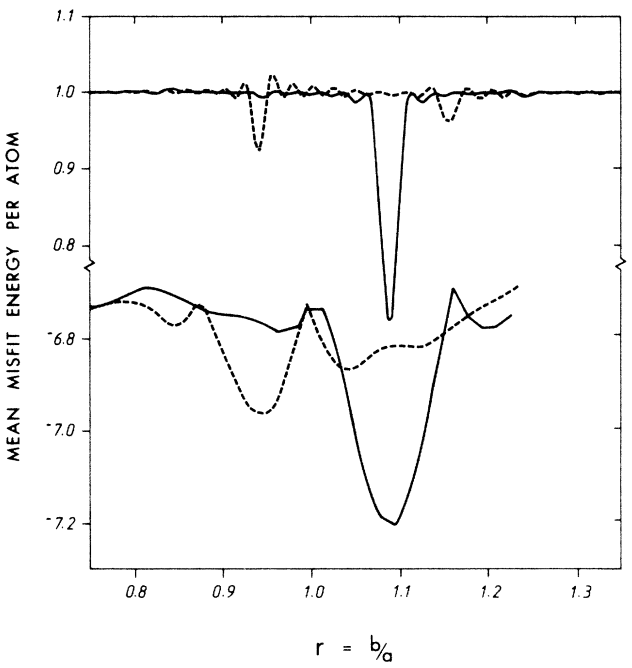

FIG. 2. Adsorbate-substrate (AS) interaction energy (mean misfit energy $\bar{v}$ per adsorbate atom) of (111) fcc or (0001) hcp monolayer with nearest-neighbor (NN) distance b on (110) bcc substrate with NN distance a, as function of the ratio $r=b/a$ for Nishiyama-Wassermann (NW) orientation (dashed lines) and Kurdjumov-Sachs (KS) orientation (solid lines) in rigid approximation (rigid monolayer and substrate). The top shows the monolayer in periodic substrate field (Ref. 6) in units of W, Eq. (B1), for a monolayer island consisting of $N=3163$ atoms. The minima become sharper as N increases. The bottom shows identical Lennard-Jones pairwise interaction potentials for layer and substrate in units of the depth of the potential well (Ref. 4).

A, as an illustration. For (111) fcc/(110) bcc interfaces (Fig. 1) with nearest-neighbor distances b and a, respectively, orientations preferred are those in which the most densely packed rows ([1$\bar{1}$0]) in the fcc (111) plane are parallel to one of the densely packed rows in the bcc (110) plane ([$\bar{1}$11],[1$\bar{1}$1],[001]).[5] The first two are called Kurdjumov-Sachs (KS) orientations, the last one the Nishiyama-Wassermann (NW) orientation. Presumably, they are most likely when the distances between the corresponding densely packed rows are the same in the two crystals. For the KS orientation this occurs when $\frac{1}{2}\sqrt{3}b=\frac{1}{3}\sqrt{8}a$ or $r\equiv b/a=1.0887\equiv r_d$, and for the NW orientation when $\frac{1}{2}\sqrt{3}b=(2/3)^{1/2}a$ or $r=0.9428\equiv r_x$ (NW-x configuration). The NW orientation is strongly preferred also when the rows perpendicular to the parallel rows in the two crystals, i.e., the fcc [11$\bar{2}$] and the bcc [1$\bar{1}$0] rows have the same distance, which is the case when $b=2a/\sqrt{3}$ or $r=1.1547\equiv r_y$ (NW-y configuration).

With increasing r, therefore, the orientation changes from NW-x to KS to NW-y at r values at which the mean energies $\bar{v}$ (per atom) of the two neighboring orientations are equal. For rigid fcc (111) monolayers on rigid bcc (110) surfaces, $\bar{v}$ was calculated by van der Merwe[6] who assumed a periodic substrate potential in the form of a truncated Fourier series, and by Ramirez *et al.*[4] who used identical Lennard-Jones (LJ) and exponential pairwise interactions between the monolayer and the substrate, which was simulated by three atomic layers. These calculations not only give information on the transitions between the various orientations but also provide an energetic justification of the geometrical selection criteria, noted above. The results are replotted in Fig. 2. As expected, the $\bar{v}$ minima coincide precisely[6] or approximately[4] with the geometrical predictions mentioned above and the r values at which the transitions between the two orientations occur differ, as seen in the figure. For the LJ potential there is actually no $\bar{v}$ minimum at r_y which, however, is obtained with the exponential potential.

The significance of these $\bar{v}(r)$ curves is not only limited by the assumption of rigidity but also by other assumptions which are far from physical reality. For example, the bcc (110) surface is inherently unstable upon minimization if modeled by LJ potentials.[7] Even with the more realistic Morse potential agreement with monolayer experiments can be achieved only if the relative magnitudes of the interaction parameters between monolayer atoms and between monolayer and substrate atoms is adjusted by an empirical correction factor.[8] Modeling the temperature dependence of the phase state of submonolayer metal films is impossible without three-body interactions.[9] Also the experimentally well-established oscillatory interplanar distances of fcc (110) surfaces cannot be explained with pairwise interaction potentials but require three-body interactions.[10] Recent Monte Carlo calculations[11] (with LJ potentials) of the maximum mismatch up to which registry between two lattices can be maintained gave a value of 15%, which is almost an order of magnitude larger than observed. As these examples indicate, calculations based on pairwise interaction potentials without *ad hoc* correc-

tion factors give no reliable quantitative information on surfaces, monolayers, and interfaces of metals. Furthermore, going beyond the rigid-lattice approximation involves an increased computational effort which is not justified in view of the limited reliability of the results.

An approach more amenable to extension beyond the rigid-lattice approximation is that in which a crystalline monolayer of atoms, with mutual elastic interaction (harmonic approximation), is exposed to the competing periodic substrate field. In the rigid approximation[6] discussed above only the mean potential energy $\bar{v}$ per atom of the unstrained monolayer in the substrate field is calculated as a function of r and θ, the relative orientation θ being measured with respect to the NW orientation. Extension to nonrigid monolayers can be made on two levels of sophistication: (i) only homogeneous strains are allowed[12] and (ii) homogeneous misfit strains (MS's) *and* oscillatory strains in the form of misfit dislocations (MD's)—frequently also called solitons or walls—are taken into consideration.[13,14] In both cases the equilibrium configuration of the monolayer is determined by the minimum, E_m, of $\bar{\varepsilon}_e+\Delta V$. $\bar{\varepsilon}_e$ is the (elastic) energy increase per atom over the unstrained monolayer ($\bar{\varepsilon}_e=0$) caused by straining, and ΔV is the change of the mean potential energy per atom above the configuration in which they are all in substrate potential minima. The most important equations are compiled in Appendix B. E_m depends essentially upon the geometry parameter $r=b/a$, the interaction parameter $l=(\Omega S/Wr^2)^{1/2}$, and the chosen strain mode: complete fit to the substrate [two-dimensional (2D) coherence, pseudomorphism $\equiv$2D C], row matching along $[1\bar{1}1]$,$[\bar{1}11]$ substrate rows [one-dimensional (1D) coherence in KS orientation $\equiv$1D KS], and row matching along [001] or $[1\bar{1}0]$ substrate rows (1D coherence in NW orientation $\equiv$1D NW-x,y), with and without misfit dislocations (MD's). Ω is the volume per overlayer atom, $S=(c_{11}^2-c_{12}^2)/2c_{11}$ (c_{11},c_{12} are stiffness constants) is a measure of the strain energy density for given strain, and W is a measure for the substrate potential amplitude and overlayer-substrate bond strength. Thus, l expresses the relative strength of intralayer to layer-substrate interactions.

With a number of simplifying assumptions, which will be discussed below, $E_m(r,l)$ may be calculated for various types of strain. Figure 3 illustrates the results for (a) strong and (b) weak layer-substrate interaction, $l\cong 3$ and $l\cong 7.2$, respectively. The data for situations involving both homogeneous strains and misfit dislocations are taken from Fig. 2 of Ref. 14(c); those for homogeneous strain only were calculated with the expressions given in Refs. 12 and 13, and the same parameters as those used in Ref. 14(c) [$P=c_{12}/(c_{12}+c_{11})=0.419$, $R=c_{44}c_{11}/(c_{11}^2-c_{12}^2)=0.939$ corresponding to Cu]. The comparison of the two sets of curves in Fig. 3 shows the influence of misfit dislocations on the minimum energy configuration (e.g., curves A and B), the comparison of Figs. 2 and 3 shows the influence of straining the monolayer. It is apparent that the allowance for straining changes the predicted orientation relationship—as is determined by minimum energy—drastically, for example by replacing the KS orientation with pseudomorphism when the layer-substrate interaction is strong (l small). The additional inclusion of MD's produces a minor correction to the stability limits, both in the analytical[14(a)] as well as in a more accurate numerical treatment[15] of the problem. Therefore, in view of the larger complexity and more limited range of validity of the calculations involving MD's,[13,14] e.g., $R=\frac{1}{2}(1-P)$ was assumed in the KS case, further

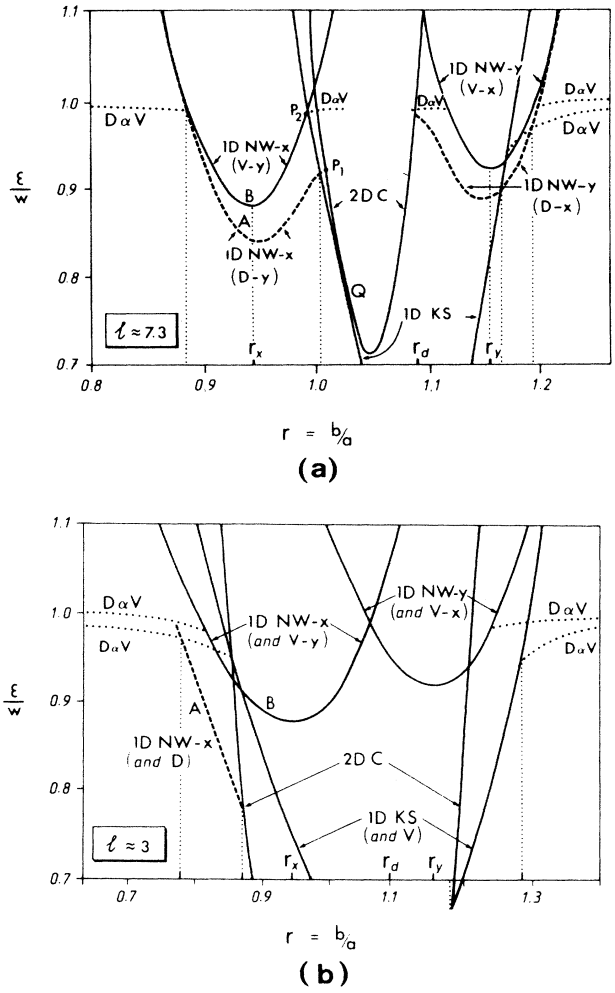

FIG. 3. Mean total (misfit and elastic) energy per atom for the same system (though elastic monolayer) as in Fig. 2, but with homogeneous (misfit) strain of 1D or 2D coherency (C) (Ref. 12) (solid curves), with C strain and oscillatory strains (misfit dislocations D) (Refs. 13 and 14) (dashed curves), and with D strains and noncoherent (vernier V) strain of the Poisson type (Refs. 12 and 14) (dotted curves). Other symbols are as follows: (i) 2D C with 2D coherency, i.e., pseudomorphy, (ii) 1D NW-x,NW-y with 1D C along $[\bar{1}10]$ or [001] bcc direction in NW orientation, (iii) 1D KS with 1D coherency along [111] or $[\bar{1}11]$ bcc directions. (a) is shown with $l\approx 7.3$ for weak AS bonding (see Appendix B), and (b) is shown with $l\approx 3$ for strong AS bonding. Vertical dotted lines indicate atomic configurations where transitions occur.

discussion will be based on the calculations in which homogeneous strains only are assumed.[12] However, some structure models derived from the calculations of Refs. 14 and 15 will be shown as an illustration of the various structures which are expected (Fig. 5).

From Fig. 3 it can be seen that the r ranges in which the various orientations (NW, KS, and pseudomorphism) are expected depend strongly on l, the relative strength of layer-layer and layer-substrate interaction. For homogeneous strain pseudomorphy should occur for $0.87 < r < 1.18$ when $l \approx 3$ but not at all when $l \approx 7.3$. The KS orientation is predicted for $1.18 < r < 1.28$ and $1.01 < r < 1.16$ in the two cases and the NW orientation for $0.78 < r < 0.88$, and $0.88 < r < 1.01$, $1.17 < r < 1.19$, respectively. A better picture of the (r,l) dependence of the preferred orientation is obtained if the regions in which E_m is smallest for the various orientations in the (r,l) plane are plotted to generate a stability or "phase diagram." This is done in Fig. 4 for the homogeneous strain case. The allowance for MD's displaces [see Eq. (B11)] the stability limits as is illustrated for the 1D NW-x configuration by the dashed line LM. Additionally the occurrence of the NW-x orientation is extended into an adjacent region (not shown) where MD's and MS's coexist (compare curve B in Fig. 3). Similar remarks apply to the NW-y and KS cases. The dotted line JK is the boundary (very crudely) between the NW-x and KS orientations as sharply defined by coherent (unstable) configurations (Appendix B). The real transitions via noncoherent configurations have a broad energy maximum.[16] An example of the atomic configurations which are predicted[14(a)] [Eqs. (B13)] for noncoherent (MD's and MS's) configurations, is illustrated in Fig. 5 for the NW-x orientation with $l=5$ [intermediate adsorbate-substrate (AS) bond strength].

When using these figures the assumptions on which their derivation rests have to be kept in mind. The assumptions concerning the monolayer are as follows. (i) Crystallinity of the monolayer: it has the same structure and equilibrium distances as in the most densely packed plane in the bulk. (ii) Only harmonic interactions occur between the atoms (linear elasticity theory). (iii) The elastic constants are the same as in the bulk. (iv) Displacements only occur parallel to the surface. For the substrate and the interaction with the monolayer the following assumptions are made: (v) The substrate is rigid. (vi) The interaction potential with the monolayer atoms is described by the first few terms of a 2D-Fourier expansion. For the Fourier coefficients, which are of great significance in the predictions, e.g., of the stability limits (see Appendix B), no reliable data are available. (vii) Electronic effects, e.g., dipole layer effects, may be neglected. (viii) Only configurations with one set of parallel dislocations are considered so that dislocation crossings in dislocation networks do not have to be taken into account. The validity of some but not all of these assumptions has been examined for special cases and in various approximations. Assumptions (i) and (iii) have been studied by using pairwise interaction potentials (Lennard-Jones and Morse)[17] and affect essentially only the precise values of r

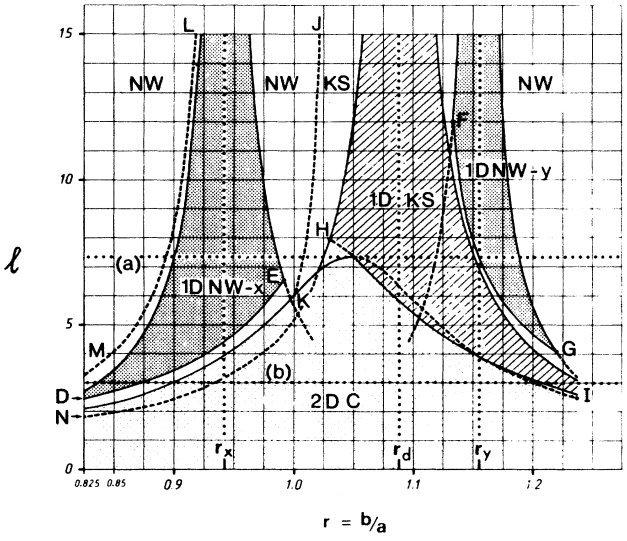

FIG. 4. Stability ranges ("phases") in (r,l) variables for pseudomorphy (2D C), 1D coherency in NW orientation (1D NW-x, NW-y) and 1D coherency in KS orientation (1D KS) of homogeneously strained (111) fcc monolayers on (110) bcc substrates with $P=0.419$ and $R=0.939$ as in Fig. 3. The dotted lines (a) and (b) represent, respectively, the cases depicted in Figs. 3(a) and 3(b). In the corridor DE, 2D C has the lower energy but is itself unstable and misfit dislocation (MD) formation (associated with curves A in Fig. 3) transforms it into a NW orientation. In the corridor FG, KS is more stable but the orientation less certain.

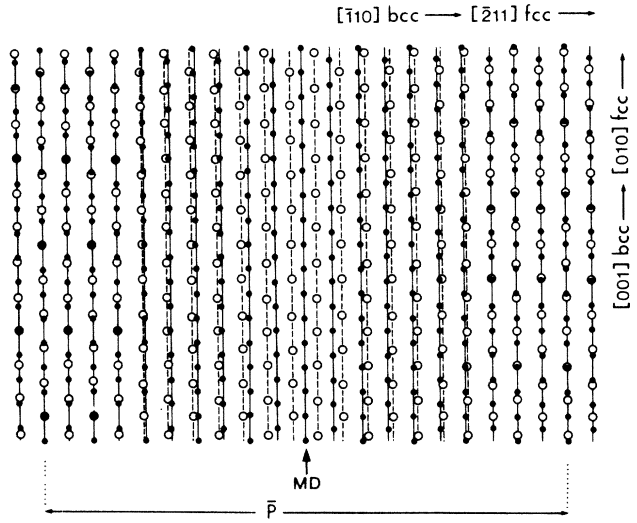

FIG. 5. Arrangements of (110) bcc substrate potential minima (○) and (111) fcc monolayer atoms (●) in the NW-x orientation for parameter values $l=5$, $r=0.837$, and MD spacing $\bar{P}=10.5a_x$ [see a_x in Fig. 1, Eqs. (B13), and D and V in Fig. 3]. In the limit $\bar{P}\to\infty$ 1D NW-x obtains. Analogous arrangements may be constructed for a KS orientation.

and l. The influence of anharmonicity (ii) has been examined for linear chains[18] using Toda and Morse potentials with the expected result that for negative misfit ($b<a$) coherence is possible over a wider misfit range than for positive misfit ($b>a$). This effect is expected to cause some minor displacements of the boundaries in Fig. 4. Assumption (v) is quite legitimate for a monolayer but becomes increasingly poorer with increasing film thickness, as will be discussed in Sec. III. Little can be said at present about assumptions (iv) and (vi)—(viii) so that the comparison with experiment (Sec. V) will have to test their admissibility.

III. TRANSITION TO MULTILAYER AND SUPERLATTICE

The transition from the monolayer to a film consisting of n layers can be made easily if the assumption is made that the rigidity modulus of the n-fold layer system may be approximated by n times the monolayer elastic constants.[19] This corresponds to a transition from l to $\sqrt{n}\,l$ in Fig. 4 and allows an immediate prediction of the evolution of the film structure with thickness. Consider for example the film-substrate combinations for which $r=r_x$, r_d, or r_y. If l is sufficiently small, then in all three cases the monolayer is predicted to be pseudomorphic. Depending on r and l, a transition to the NW-x (r_x) or KS orientation (r_d) may occur when the second monolayer forms ($l_2=\sqrt{2}l$) and this orientation will persist with further film growth. For $r=r_y$ the situation is more complicated: For an appropriate l the double layer ($l_2=\sqrt{2}l$) will have the KS orientation, and an n-fold layer (n large enough) film the NW orientation, provided kinetic limitations do not suppress the transition. If MD's are taken into account (Fig. 3), such orientation changes are possible over a wider r range. For example, below $r\approx 1.0$ there will be a transition via misfit dislocations to the 1D NW-x orientation if the present values of the Fourier coefficients are accurate enough. If A_1 and A_2 in (B1) and (B5) were large enough, the line KN would lie above ED and the transition would occur via a KS orientation. Clearly the transitions are more complex if r differs significantly from the ideal values r_x, r_y, or r_d. These examples show that it is, in general, not possible to conclude from the monolayer structure alone what structure a multilayer should have and (as regards this matter) the interaction parameter l may play a decisive role.

In the transition from the multilayer to the superlattice two additional considerations come into play. One concerns the crystallinity. The KS orientations occur in two equivalent orientations ([1$\bar{1}$0] fcc ||[111],[11$\bar{1}$] bcc). A single B multilayer on a single crystalline A substrate may, therefore, still be considered quasicrystalline. Each substrate A or B multilayer stack adds additional azimuthal orientations so that with increasing number of stacks the system increasingly breaks up into equivalent azimuthal orientations and loses it superlattice crystallinity as defined in the Introduction. An additional complication is that alternate stacks emanate from a (111) fcc rather than a (110) bcc substrate. The Fourier component which generates a given orientation, e.g., one-dimensional (1D) NW-x, is thus different. In fact, calculations[16] show that the 1D NW-y orientation on a (111) fcc substrate only appears at higher-order Fourier components. Thus, A-B multilayer pairs in KS orientation are unsuitable for superlattice growth as already noticed by Ramirez *et al.*[4] unless the equivalence of the two orientations is eliminated.

The second consideration concerns the assumptions (i) of a rigid substrate and (ii) that there is no strain gradient normal to the film plane. While these assumptions are reasonable for a thin film on a thick substrate, this is not the case any longer when substrate A multilayer stack and film B multilayer stack are of comparable thickness, particularly when A is elastically less stiff than B. The strains are then distributed in A and B multilayers in relative amounts depending upon elastic constants and thickness. The AB interfacial energy is accordingly decreased relative to that with a rigid substrate to create conditions more favorable to layer-by-layer growth. The magnitude of the energy reduction can be estimated[20] from model calculations, for rectangular lattices with misfit in one direction only, as less than 10%.

IV. THE GROWTH MODE

In the preceding sections it has been tacitly assumed that the geometrical constraint of plane-parallel growth, which is a prerequisite for superlattice formation, can be realized under the quasiequilibrium conditions which are necessary in order to allow the growing film to approach good crystalline order. This assumption however, is not correct in general (Appendix C). Thin crystalline films grow near equilibrium by one of three mechanisms:[21] the Vomer-Weber (VW), the Stranski-Krastanov (SK), and the Frank—van der Merwe (FM) mode, depending upon the relative magnitudes of the surface energies. γ_s,γ_f of the substrate and the film, respectively, and of the interfacial energy γ_{in}. Monolayer-by-monolayer growth occurs only in the FM mode which obtains when $\Delta\gamma_n=\gamma_{fn}+\gamma_{in}-\gamma_s\leq 0$ for all n, i.e., independent of thickness.[21] Here the n-dependent strain energy in the film has been absorbed in γ_{in}. γ_f and γ_s are the values for the semi-infinite crystals, and $\gamma_{\rm fn}$ deviates somewhat from γ_f due to the n-dependent surface strain. The condition is rigorously fulfilled only for the growth of A on A (homoepitaxy) in which case $\gamma_f\equiv\gamma_s$ and $\gamma_{in}\equiv 0$, or more generally for zero misfit, i.e., when the strain contribution $\gamma_{in}^{\varepsilon}$ to γ_{in} is zero and $\gamma_f+\gamma_{in}^0-\gamma_s\geq 0$. Here γ_{in}^0 is the zero strain contribution to γ_{in} which depends on the specific chemical interaction between film and substrate atoms and rapidly approaches zero within the first few monolayers, depending upon the range of the interatomic forces.

In all other cases the increase of the strain energy with n leads to an increase of γ_{in} until at a given $n=n^*$ the FM condition is not fulfilled any longer and three-dimensional crystals form (SK mode). If the FM condition is not fulfilled from the very beginning ($n=1$), then three-dimensional crystals form immediately on the sub-

strate (VW mode). These three growth modes have subsequently[22] also been called class I, II, and III behavior for the FM, SK, and VW modes, respectively, and have recently been studied in great detail in the theory of wetting and layering transitions as complete wetting, incomplete wetting, and nonwetting cases (see, for example, Refs. 23–25 and references therein).

Here it is only important to note that FM (class I, complete wetting) growth which is desired in superlattice growth occurs only under rather restricted conditions: (i) γ_f should be smaller than γ_s, and (ii) γ_{in} should be small. These conditions should be fulfilled both for the growth of B on A and of A on B which obviously is not possible for condition (i). Thus a true FM growth mode cannot be achieved in the growth of superlattices but can only be approached when $\gamma_A \approx \gamma_B$ and γ_{in} is small. Whenever γ_A and γ_B differ strongly, the metal with the larger γ will form three-dimensional crystals which suppresses superlattice formation. This difficulty can be alleviated somewhat by giving up quasiequilibrium conditions and going to higher supersaturations $\Delta\mu = \mu - \mu_0$ (μ_0 equilibrium chemical potential) by increasing the deposition rate or decreasing the substrate temperature. In this manner the nucleation rate of the three-dimensional crystals in the SK mode and even in the VW mode can be made so large that they merge into a continuous multilayer before the desired thickness is reached.

This pseudo-FM mode which is induced by limited mobility and high nucleation rate is distinctly different from the supersaturation-induced true FM mode which has been derived erroneously,[26,27] as discussed in Appendix C. In this mode the critical nucleus height decreases with increasing $\Delta\mu$ to the thickness of a monolayer at a critical $\Delta\mu = \Delta\mu_c$ which is proportional to $\Delta\gamma$. For all $\Delta\mu \geq \Delta\mu_c$ the true FM mode should prevail. If this were the case, superlattices with an arbitrarily large number of AB sequences could be grown without noticeable increase in interface roughness. In the absence of this mechanism a certain roughness increase is unavoidable. Fortunately, the interface energy tries to minimize the interface area. Thus, if the experimental conditions are chosen in such a manner as to allow rearrangements on an atomic scale during interface formation the interface will become smoother so that sufficiently thick superlattices can be grown (see Appendix C).

The considerations above suggest that the ease with which superlattices may be grown from the point of view of the surface energy, may be characterized by a compatibility factor, the "surface energy mismatch"

$$\Gamma_{AB} = 2\,|(\gamma_A - \gamma_B)/(\gamma_A + \gamma_B)|\ .$$

With the γ values of Ref. 28 one obtains from the still sparse experimental data (Cu/W, Cu/Mo, Cu/Nb; Ni/W, Ni/Mo, Ni/V) (Ref. 4) a critical value $\Gamma^c_{AB} \approx \frac{1}{2}$. For $\Gamma_{AB} < \Gamma^c_{AB}$ superlattice formation should be possible and for $\Gamma_{AB} > \Gamma^0_{AB}$ it should not. The value $\Gamma^c_{AB} = \frac{1}{2}$, together with Fig. 4, will be used in Sec. VI to predict the feasability of superlattice growth. First, however, the reliability of Fig. 4 will be examined by comparison with monolayer and multilayer experiments.

V. COMPARISON OF THEORY AND EXPERIMENT FOR MONOLAYERS AND MULTILAYERS

There are several recent comparisons between theoretical predictions of epitaxial orientations and growth modes and experiment[29,30] in which references to the original work can also be found. Therefore, only a few selected examples, distributed over the (r,l) range of Fig. 4, and some new results, to be published in detail elsewhere, will be discussed. Be on W ($r=0.812$, $l \sim 5$ assuming $W=0.1$ eV) should have the NW orientation in the first monolayer, which is confirmed by experiment.[29] Although $\gamma_{Be} = 1.12$ J/m^2 $\ll \gamma_W = 3.47$ J/m^2 (Ref. 28) so that multilayer formation is possible, a double layer is unstable and so MD's form, and the onset of SK growth becomes more likely. With the transition, a regrouping of atoms into crystallites with a change of orientation is probable. The formation of a double layer (with KS orientation according to Fig. 4) is thus less favorable than the growth of flat three-dimensional (3D) crystallites.[29] These crystals do not have a (0001) plane parallel to the substrate but have a $(10\bar{1}0)$ plane which has a small misfit with the substrate. The next largest b/a ratio studied, Cu/Nb (Ref. 31) ($r=0.894$) shows in thick films the NW orientation, like all other systems up to $r=0.963$ (Pd/Nb).[31,32] Quasi-FM growth is seen in all cases at room temperature while at elevated temperatures there is SK growth, usually with two monolayers before three-dimensional nucleation occurs. This may also be understood in terms of a transition from a metastable coherent state to a stable noncoherent state with MD's, the higher temperature providing the activation for the motion/generation of MD's. In pairs which can form alloys [Ni/W (Ref. 33), Mo (Ref. 31), Nb; Co/W (Ref. 31), Pd/Ta, Nb (Ref. 32)] alloying occurs above 700–800 K. In the range 0.894 [(Cu/Nb) (Ref. 31)] $\leqq r \leqq 0.915$ [(Co/W) (Ref. 31)] the first monolayer grows pseudomorphic up to about one substrate monolayer and then changes within this first monolayer into a coincidence structure with an atomic distribution very similar to a (111) plane in NW orientation. Already in the second to third monolayer the lattice spacings are indistinguishable from the bulk values. In the range 0.933 [(Cu/W) (Ref. 31)] $\leqq r \leqq 0.963$ [(Pd/Nb) (Refs. 31 and 32)] the reorganization of the first monolayer into the coincidence structure coincides with the beginning of the second monolayer. The increase in the stability of the pseudomorphic layer with increasing r is in full agreement with the stability diagram (Fig. 4) and so is the NW orientation of thicker layers in this r range.

The switchover from NW to the KS orientation is seen for the first time at $r=0.992$ (Ru/Mo) (Ref. 31), but it is not certain in this case that no alloying occurred at the interface. Clear boundary cases are Pd/W (Refs. 29 and 31) ($r=1.004$) and Pd/Mo (Ref. 34) ($r=1.009$). At room temperature quasi-FM growth in NW orientation is observed which is considerably strained initially and preceded by a strained pseudomorphic monolayer. At elevated temperatures ($T \gtrsim 700$ K) SK growth preceded by a pseudomorphic (on W) or incommensurate monolayer (on Mo) occurs. An alloy transition layer is probably responsible for this difference in orientation, but it should be noted

that $r=1$ is at the border between NW and KS orientations, so that changes in the deposition conditions may cause one or the other orientation to appear. Unfortunately, the r range in which the KS orientation is expected (see Fig. 4) has been studied only up to $r=1.060$ (Ag/Mo) (Refs. 31 and 35). In all cases which have been studied in sufficient detail (Ag, Au/W,Mo) (Refs. 31, 35, and 36), quasi-FM growth is seen at room temperature and SK growth with one to three stable monolayers is seen at high temperatures ("quasiequilibrium conditions"). Again, a higher-temperature provides activation energy for MD formation and motion to create conditions more favorable for SK growth (see Appendix C). The structure of the first two layers is usually quite complex as is well illustrated in the Au/W system,[36] in contradiction with the theoretical predictions of Fig. 4.

Above $r=1.06$ there is a large jump to 1.162 (Fe/Au) (Refs. 37 and 38) in the r values studied reliably. Although in general the NW orientation is observed,[37,38] the KS orientation has also been reported.[38] The situation is complicated by alloying at elevated temperatures (≥ 300 °C) (Ref. 37) but in the immiscible system Fe/Ag (Ref. 39) ($r=1.164$) only the NW orientation occurs. The boundary must therefore be between $r=1.06$ and $r=1.16$. This differs somewhat from the predictions embodied in Fig. 4 and may imply that the Fourier coefficients A_1 and A_2 associated with the KS orientation have been overestimated relative to that (A_4) associated with the NW-y orientation. The NW stability range for thick layers has been confirmed by experiment up to $r=1.376$ (La/Mo).[3] The pseudomorphism predicted for the first monolayer does not occur, mainly for two reasons: (i) all layers in this r range [Sc (Ref. 3), Tb (Ref. 39), Gd (Ref. 39), Y (Ref. 3), La (Ref. 3), and even Pb (Ref. 3)] have repulsive lateral interactions in the first monolayer which cause ordered superstructures, and (ii) the anharmonicity of the interaction potential makes compressive strains much less favorable and therefore causes an asymmetry in the pseudomorphy boundary line which is not accounted for in Fig. 4. Except for Pb which grows in the SK mode already at room temperature, the layers show the temperature-dependent growth behavior as described before.

It should be pointed out that the preceding description gives a somewhat simplified picture. The initial growth (first monolayer) depends, at least in some systems, sensitively upon the perfection of the surface [Cu/Mo, Ni/Mo (Refs. 29, 31, and 35)] and is strongly influenced by chemical surface modifications such as oxygen or carbon adsorption [Au/Mo (Ref. 31)]. These effects can cause and actually have caused considerable differences between different studies of the same film/substrate pairs. The data reported above are for the cleanest conditions presently obtainable (deposition and investigation in the 10^{-11} torr range).

From these examples and other comparisons between theory and experiment[29,30] the following conclusions may be drawn: (i) Within its applicability range theory (Fig. 4) predicts semiquantitatively the observed orientation of monolayers and multilayers—provided multilayers form at all. In particular it shows that at most one pseudomorphic monolayer can form for interaction parameter (l) values of interest in superlattices. At least the double layer already has the orientation predicted for the particular r,l combination. Differences between theory and experiment in the monolayer orientation (e.g., for Ag and Au on W and Mo) may be due (a) to an overestimation of the amplitude of the surface potential which is proportional to W, resulting in too low an l value, (b) to neglect of anharmonic effects which make compression ($b>a$) into the pseudormorphic state less favorable than the KS orientation or, (c) to specific electronic effects which frequently occur in the monolayer substrate interaction. (ii) In many cases, in particular when r differs notably from the optimal values r_x, r_d, and r_y (E_m large), only one or two monolayers are formed under quasiequilibrium conditions, followed by three-dimensional crystal growth (SK mode). This is mainly due to the rapid increase of the strain energy resulting in an instability of the multilayer with respect to the formation of MD's and the development of conditions favorable to SK growth for n as small as 2 or 3. In some cases however, such as in Pd and Ni on W, electronic effects which are evident in the abnormal work function at monolayer coverage are responsible for poor wetting of the first or second layer by the subsequent layers. (iii) Even if SK growth prevails under quasiequilibrium, pseudo-FM growth can be obtained at a sufficiently low temperature, which in many cases is room temperature. Conclusions (ii) and (iii) show that even when $\gamma_f \ll \gamma_s$, so that $\Delta\gamma_n \leqq 0$ is true initially, pseudo-FM growth conditions are necessary in order to obtain films with low roughness.

VI. CONCLUSIONS FOR SUPERLATTICE STRUCTURE AND GROWTH

Two basic conditions must be fulfilled in the growth of crystalline superlattices: (i) There may be only *one* orientation relationship between the two components and (ii) the surface energies of the two component metals must be compatible. Condition (i) must be formulated somewhat more precisely as the following analysis of the NW orientation shows. This orientation is unique for fcc (111) on bcc (110), except for the stacking sequence in the fcc (111) which may grow *abc* or *acb* leading to twinning. After the completion of the fcc (111) stack the new substrate has three equivalent $\langle 110 \rangle$ directions—unless the stack is so thin that the original substrate potential is still replicated in the strain distribution—so that three equivalent NW orientations rotated $2\pi/3$ with respect to each other grow. No additional orientations are formed upon further superlattice growth because the already existing orientations repeat due to the fact that the rotation angle is a rational fraction of 2π. For other rational fractions more stacks may be necessary before the full manifold of azimuthal orientations has developed. For nonrational fractions of 2π—for which the KS orientation with $\theta=5.26°$ is an example—no orientation saturation occurs, with increasing number of stacks leading to layered, i.e., azimuthally unoriented growth. Thus it is apparent that a more concise form of condition (i) is that the orientation must be such that the orientation-determining axes in the interface

between the two components enclose only angles which are rotational fractions of 2π ("angular commensurability").

Concentrating on fcc (111)/bcc (110) pairs only, partners with r values leading to the NW orientation are suitable for crystalline superlattice formation. For a selection of metal pairs [including hexagonal metals with hcp (0001) layers] the r values are shown in Table I. There are a few boundary cases which are uncertain due to the uncertainty in the l values. The Γ_{AB} values which are also shown in Table I indicate to what extent condition (ii) is fulfilled. It should be noted that only the surface energy mismatch Γ_{AB} was taken into account and that the inclusion of the interfacial energy γ_i may eliminate some metal pairs as superlattice partners. Alloying or compound formation at an interface with given misfit, essentially increases the interfacial bond strength and accordingly the stability against MD formation, i.e., enhances the tendency towards desirable FM growth. Of course, in order to obtain a sharp interface the temperature has to be so low that place exchange between "film" and "substrate" cannot occur. These temperatures are much lower, due to the enhancement by strains and grain boundary diffusion, than the diffusion temperatures used with bulk samples. This is amply demonstrated in many thin film interdiffusion studies.

It is evident from Table I that the surface energy mismatch criterion limits the pairs suitable from the orientation point of view significantly, mainly to alloy (and compound forming) systems. In particular, the system Cu/W, which was not understood in previous work, is excluded. In this system the W particles are probably covered immediately with a Cu skin at the deposition temperatures used so that they cannot form a continuous W layer despite their small size. All observed superlattices[4] (Ni/V, Ni/Mo, Ni/W, Cu/Mo, Cu/Nb) are highly favored by both criteria. Figure 4 also predicts crystalline superlattice formation for Ni/Nb, in contradiction with experiment,[4] a discrepancy probably due to alloying. This may also be the case for Cu/V which is close to the border between the NW and KS orientations. In view of the uncertainty of the γ values of rare earths, A-B pairs involving them are highly questionable. Whenever the values are certain, the predictions should be too, within the limitations mentioned before, so that Fig. 4 should be a reliable guide for experiments.

VII. SUMMARY

In this paper the basic factors which determine the growth and structure of metallic superlattices were discussed and the conditions for superlattice growth were derived so that in the future unnecessary empirical studies in this rapidly expanding field can be avoided. The most important factors are the uniqueness of the epitaxial orientation relationship and the surface energy compatibility. It was shown that for fcc (111)/bcc (110) interfaces the orientation can be predicted with a high degree of reliability with uncertainties only in the boundary regions between different orientation relationships. Unless special experimental conditions are chosen, unique orientations necessary for crystalline superlattice growth are obtained only in certain ranges of the ratios $r=b/a$ of the atomic diameters of the superlattice components. Outside these ranges, where two equivalent orientations occur, the use of unidirectional stepped substrate surfaces and of deposition conditions which lead only to nucleation on steps may make crystalline superlattice growth possible too. The orientation changes which occur with increasing thickness as predicted by misfit dislocation theory, do not seem to occur according to the presently available experimental evidence. This is due to the fact that it is energetically more favorable to form three-dimensional crystals with small interface than to continue the growth of a highly strained quasi-two-dimensional multilayer film.

The three-dimensional growth of metals with high surface energy on metals with low surface energy is the main factor limiting to superlattice growth. It makes it impossible to grow crystalline and—in extreme cases—even layered superlattices. When the surface energies are less incompatible, superlattices with acceptable crystalline quality may be grown at sufficiently low temperatures and high supersaturations but quantitative predictions cannot be made at present because the necessary quantities such as interfacial energies, and in some cases even surface energies, are not known at all or not accurately enough. Nevertheless the qualitative predictions of r_{AB} and Γ_{AB} ranges which are possible, given the present knowledge of the relevant quantities, allows the exclusion of a large number of metal combinations so that experimental studies can concentrate on the feasible combinations. Future theoretical work will have to be based on more realistic surface potential calculations (Fourier coefficients and absolute value W) so that the orientation can be predicted more reliably in the border regions. Future experimental work will have to generate reliable values of the still unknown surface and interfacial energies in order to allow selection of compatable metal pairs.

ACKNOWLEDGMENTS

Most of the work of one of the authors (E.B.) was done while he was a guest at the University of Pretoria. He is very grateful to J. H. van der Merwe and to the University of Pretoria for their hospitality and for financial support. Numerical calculations and plots by Mr. M. Braun are appreciated. One of the authors (J.H.v.d.M.) gratefully acknowledges financial support from the Council for Scientific and Industrial Research Foundation for Research Development.

APPENDIX A: GEOMETRICAL ORIENTATION SELECTION CRITERIA FOR fcc (111) AND hcp (0001) INTERFACES

Compared to the bcc (110)/fcc (111) interfaces, these interfaces have received relatively little attention. Therefore, we use them to illustrate the geometric considerations. They are based on the coincidence principles which are as old as epitaxy research is. If $\mathbf{a}_i$ $(i=1,2)$ are the unit mesh vectors in the substrate surface and $\mathbf{b}_i$ are those of the film, then the two-dimensional coincidence condi-

TABLE I. Geometry parameter $r=b/a$ and surface energy mismatch $\Gamma_{AB}=2|(\gamma_A-\gamma_B)/(\gamma_A+\gamma_B)|$ for various fcc (hcp)/bcc metal pairs. The first horizontal (vertical) row gives the atomic diameters a (b) in Å, the second the surface energy at room temperature in Jm^{-2} (Ref. 28). The first number in the table is r_{AB}, the second Γ_{AB}. For superlattice formation Γ_{AB} should be less than about $\frac{1}{2}$, for *crystalline* superlattice formation $r_{AB}\lesssim 1.00$ or $\gtrsim 1.15$. Combinations for which crystalline superlattice growth experiments were successful or unsuccessful (Ref. 4) are underlined or enclosed in parentheses, respectively.

			A													
			Cr		V		Mo		Fe		Nb		Ta		W	
			2.498		2.619		2.726		2.482		2.858		2.863		2.741	
	B		2.056		2.876		2.877		2.939		2.983		3.018		3.468	
Gd	3.636	0.935	1.455	0.750	1.388	1.019	1.334	1.019	1.465	1.035	1.272	1.045	1.270	1.054	0.326	1.151
La	3.75	1.055	1.501	0.644	1.432	0.926	1.376	0.927	1.511	0.943	1.312	0.955	1.310	0.964	1.368	1.067
Y	3.647	1.160	1.303	0.557	1.393	0.860	1.338	0.851	1.469	0.868	1.276	0.880	1.274	0.889	1.330	0.997
Ag	2.889	1.302	1.157	0.449	1.103	0.753	1.060	0.754	1.164	0.772	1.011	0.785	1.009	0.794	1.054	0.908
Au	2.884	1.626	1.154	0.234	1.101	0.555	1.058	0.556	1.162	0.575	1.009	0.589	1.007	0.599	1.052	0.723
Cu	2.556	1.934	(1.023)	(0.046)	(0.976)	(0.392)	0.938	0.392	(1.030)	(0.412)	0.894	0.427	0.893	0.437	(0.933)	(0.568)
Pd	2.751	2.043	1.101	0.006	1.050	0.339	1.009	0.339	1.108	0.360	0.963	0.374	0.961	0.385	1.004	0.517
Ni	2.492	2.364	(0.998)	(0.139)	0.951	0.195	0.914	0.196	1.004	0.217	(0.872)	(0.231)	0.870	0.243	0.909	0.379
Pt	2.774	2.691	1.110	0.267	1.059	0.066	1.018	0.067	1.118	0.088	0.971	0.103	0.969	0.115	1.012	0.252
Co	2.507	2.790	1.004	0.303	0.957	0.030	0.920	0.031	1.010	0.052	0.877	0.069	0.876	0.078	0.915	0.217
Rh	2.689	2.828	1.076	0.316	1.027	0.017	0.986	0.017	1.083	0.038	0.941	0.053	0.939	0.065	0.981	0.203
Re	2.761	3.109	1.105	0.408	1.054	0.162	1.013	0.077	1.112	0.056	0.966	0.041	0.964	0.030	1.007	0.109
Ir	2.715	3.231	1.087	0.444	1.037	0.116	0.996	0.116	1.094	0.093	0.950	0.080	0.948	0.068	0.990	0.071
Ru	2.704	3.409	1.082	0.495	1.032	0.170	0.992	0.169	1.089	0.148	0.946	0.133	0.944	0.122	0.987	0.017

tion is $N_i\mathbf{b}_i=\sum_{k=1}^{2}n_{ik}\mathbf{a}_k$ $(i=1,2)$, where the n_{ik} and N_i are integers and the $N_i\mathbf{b}_i$ the unit mesh vectors of the superlattice formed by the coincidence. For the interfaces considered here, film and substrate have the same symmetry and the $\mathbf{a}_i$ and $\mathbf{b}_i$ enclose the same angles (60°). The $\mathbf{b}_i$'s may be rotated relative to the $\mathbf{a}_i$'s by an angle $\alpha_i\equiv\alpha$ ("rotational epitaxy") and for symmetry reasons $N_1=N_2=N$. Therefore, the orientation is completely determined by specifying one superlattice unit mesh vector, say $N\mathbf{b}_1=n_1\mathbf{a}_1+n_2\mathbf{a}_2$. From its inner product one obtains

$$r^2=\left[\frac{b}{a}\right]^2=\frac{n_1^2+n_1n_2+n_2^2}{N^2},$$

with $|\mathbf{a}_1|=|\mathbf{a}_2|=a$ and $|\mathbf{b}_1|=b$, and from the vector product with $\mathbf{a}_1$ the sine of the rotation angle

$$\sin\alpha=\frac{\sqrt{3}}{2}\frac{n_2}{(n_1^2+n_1n_2+n_2^2)^{1/2}}.$$

For a given unit mesh dimension b_0 of the film the ratio $(b_0/a)^2$ can be mathematically approximated arbitrarily well by sufficiently large (N,n_1,n_2) values. However, physical limitations—atomic perfection of the substrate over distances of several Nb, and kinetic difficulties in attaining the complex long-range order—set an upper limit to N which is determined by the experimental conditions. Nevertheless, there are always several (N,n_1,n_2) combinations which lead to b/a values close to b_0/a so that coincidence can be achieved by a small homogeneous strain $e=(b-b_0)/b_0$. An additional complication is that the equilibrium structure, the equilibrium spacing b_e in particular, of a monolayer on a flat, laterally noninteracting substrate will almost certainly differ[16] from the bulk value b_0. Which of the various (N,n_1,n_2) combinations will occur can again only be decided by energy calculations such as those which have been made in connection with the rotational epitaxy of noble gases on graphite.[38–41] They require a detailed knowledge of the interactions and are beyond the scope of this paper.

Here we compare only the selected experimental results shown in Table II with the geometrical predictions. It is evident that all the observed orientations can be explained by parallel or rotated coincidence lattices with small strains. There are, however, for a given b_0/a value, usually other (N,n_1,n_2) combinations with small commensurability number N and comparable or even smaller strain. In some cases the absence of the better fitting coincidence lattice may be attributed to the anharmonicity of the intralayer interactions which favors dilation relative to compression. An example is Ag/Cu, where a much smaller but compressive strain ($e=-0.44\%$), would be obtained with a (8,9,0) coincidence lattice. In other cases such a simple explanation is not possible. Thus for Pb/Al $e=-0.05\%$ and for Pb/Ag $e=-0.21\%$ for the unrotated coincidence lattices (9,11,0) and (14,17,0), respectively. This shows that a justification for the selection of the observed orientation from several possible low N coincidence lattices is not possible by geometrical considerations alone, but requires a full scale energy calculation which properly takes account of longitudinal and transverse components of the distortions. How subtle the effects are is illustrated by the Cu/Ru system. On a very perfect Ru(0001) surface a rotated Cu monolayer is observed[47] which can be explained by a coincidence lattice with very large unit mesh ($29d_{Cu}=74$ Å). On a less perfect surface Cu grows in parallel orientation with a much smaller coincidence distance ($18d_{Cu}=46$ Å) and strain (-0.01% versus $+0.33\%$).[48] It should be noted that in the former case the rotation is limited to the monolayer while thicker films also grow in parallel orientation.[47]

The lattice rotation in metal layers in which the lateral interactions are attractive is closely related to the rotational epitaxy in adsorbed monolayers with repulsive lateral interactions. In these systems the lattice constant can be varied continuously over a limited coverage range with concomitant changes of the rotation angle. Table II shows the (N,n_1,n_2) values for some of the (r,α) combinations observed in physisorbed Ne (Ref. 49) and Ar (Ref. 50) layers on the graphite basal plane. A much wid-

TABLE II. Orientation relationships of hexagonal interfaces. N,n_1,n_2 are the theoretical values which give the best fit to the observed orientations α_{exp}, which agree within the limits of the experimental error with the calculated α shown in the table. e is the strain necessary in order to achieve coincidence. N is called here commensurability number in contrast to the one-dimensional case ($n_2=0$) in which this expression is used for n_1.

Film/substrate	$r_0=\frac{b_0}{a}$	N	n_1	n_2	α (deg)	e (%)	Expt. Ref.
Pb/Ni	1.405	5	7	0	0	−0.35	44
Pb/Cu	1.370	3	4	0	0	−2.68	44
Pb/Al	1.222	9	10	2	9.02	+4.40	44
Pb/Ag	1.212	19	22	2	4.31	−0.01	44,45
Ag/Ni	1.159	6	7	0	0	+0.63	44
Ag/Cu	1.130	7	8	0	0	+1.11	44
Cu/Ru	0.945	29	27	1	1.80	+0.33	46
Cu/Ru	0.945	18	17	0	0	−0.01	47
Ne/C	1.281	9	9	4	17.48	0	48
Ar/C	1.559	18	27	2	3.54	0	49
Ar/C	1.608	14	22	1	2.20	0	49

er range of (r,α) combinations can be obtained in chemisorbed layers. These layers may be considered as consisting of rows of atoms parallel to the close-packed substrate directions. The decrease of the atomic distance with increasing coverage is made as isotropically as is compatible with the substrate symmetry by a simultaneous shift of the adjacent rows which changes the rotation angle. The rotation reported recently for Na/Ru(0001) (Ref. 51) is a special case of the more general situation seen in film-substrate combinations with different symmetry such as Pb/W(110) (Ref. 52) or Te/W(110) (Ref. 53). On the bcc (110) surface the row shift occurs along the $[1\bar{1}1]$ or $[\bar{1}11]$ direction and causes not only a change of α but also of the unit mesh shape due to the symmetry difference. The hexagonal Na layer on the hexagonal Ru(0001) surface maintains its unit mesh shape during the row shift parallel to the $\langle\bar{1}10\rangle$ directions ("30° trajectory") (Ref. 51) and changes only its rotation angle. In some systems of interest for metallic superlattices such as pairs involving rare earths (e.g., Gd) (Ref. 40) the rotation is not continuous. Inasmuch as these discontinuous rotations always occur on the submonolayer range and terminate in a fixed value at monolayer saturation, they will not be discussed here further because they are not relevant to the question of whether or not for a given A-B pair a crystalline superlattice may be grown, that is whether or not α is a rational fraction of 2π.

The comparison between geometrical considerations and experimental observation demonstrates that for a given $r_0=b_0/a$ there are in general various α values which give good coincidence. A reliable prediction on geometrical grounds is therefore not possible. It appears that, at the present knowledge of the atomic interactions on metal surfaces and with the available computational tools, a prediction on energetic grounds will also be rather limited if one takes the subtleness of the effects into account (Cu/Ru). Therefore, for the time being it remains for the experiment to determine the suitability of a given A-B combination for crystalline superlattice growth. In this determination it must be kept in mind that α depends upon the perfection of the surface and may be different between monolayer and thicker film (Cu/Ru).

APPENDIX B: EPITAXY AND MISFIT ACCOMMODATION IN MONOLAYERS

A model for the description of the behavior of a monolayer adsorbate (adatoms) on a crystalline substrate surface (CSS) must provide for adsorbate-substrate (AS) and adsorbate-adsorbate (AA) interaction, and for the principles governing its formation and stability. It has been assumed *firstly*[19,54] that the AS interaction has the periodicity and symmetry of the CSS, for a single adatom as well as for a completed monolayer or multilayer, and *secondly*, that it may be adequately approximated by a truncated Fourier series. In order that the model predicts[6,14] the observed NW and KS orientations truncation at the second harmonic terms are needed. Thus for the (110) bcc CSS

$$
\begin{aligned}
V(x,y)=W\Bigg\{&A-A_1\cos\left[2\pi\left[\frac{x}{a_x}+\frac{y}{a_y}\right]\right]\\
&-A_2\cos\left[2\pi\left[-\frac{x}{a_x}+\frac{y}{a_y}\right]\right]\\
&-A_3\cos\left[4\pi\frac{x}{a_x}\right]-A_4\cos\left[4\pi\frac{y}{a_y}\right]\Bigg\},\\
&A_1=A_2=0.4,\quad A_3=0.12,\quad A_4=0.08,\\
&A=A_1+A_2+A_3+A_4=1,\\
&a_x=2a\sin\alpha,\quad a_y=2a\cos\alpha,\quad \alpha=\arctan(2^{1/2}),
\end{aligned}
\tag{B1}
$$

where the axes and the lengths a_x and a_y are shown on the rhombic unit cell $PQRS$ of the (110) bcc CSS in Fig. 1, the origin (0,0) being at an energy minimum. Quantitatively the A_i are based on qualitative arguments, no quantitative data being available. An additional assumption,[6]

$$
E_{\text{diff}}=\kappa E_{\text{des}},\quad 0.1\lesssim\kappa\lesssim 0.33,
\tag{B2}
$$

relates the activation energy E_{diff} for adatom surface migration to the adatom desorption energy (AS bond strength) E_{des}. The relevant value of κ depends on AS bondtype and CSS atomic arrangement. With relation (B1),

$$
W=E_{\text{diff}}/1.2,
\tag{B3}
$$

whereby the parameter W becomes an approximate measure of AS bond strength in this analysis.

The AA interaction is assumed[13] to, *firstly*, induce 2D quasicrystallinity in the adsorbed closely packed monolayer (on a flat structureless substrate) with a unit cell which is usually approximated by the corresponding bulk unit cell, and normally does not match that in the CSS, and *secondly*, to behave according to the harmonic approximation when the 2D crystal is deformed by the competing AS interaction (B1). The resulting elastic strain energy per adatom is of the form[6,13]

$$
\begin{aligned}
&\varepsilon=Wl^2r^2(e_x^2+e_y^2+2Pe_xe_y+Re_{xy}^2),\quad r=b/a\\
&l^2=\frac{\Omega S}{Wr^2},\quad S=\frac{c_{11}^2-c_{12}^2}{2c_{11}},\\
&P=\frac{c_{12}}{c_{12}+c_{11}},\quad R=\frac{c_{11}c_{44}}{c_{11}^2-c_{12}^2},
\end{aligned}
\tag{B4}
$$

where the e's and c's are, respectively, the strain components and stiffness constants for cubic crystals, and Ω the volume per adatom. Also a more refined analysis,[16] using transformed stiffness constants, changes the formulas for P, R, and S somewhat, but has negligible consequences on the results.

The calculations have been limited[6,13] to ground-state (zero-temperature) configurations obeying minimum energy principles, and invoked the temperature only implicitly for the acquisition of equilibrium. The equilibrium (stable) configurations are characterized by homogeneous

(misfit) strain (MS), oscillatory strains or misfit dislocations (MD's) and an epitaxial orientation angle θ. θ is conveniently chosen as $\theta_{NW}=0$ and

$$\theta_{KS}=60-\arctan 2^{1/2}\simeq 5.3^\circ$$

in the NW and KS orientations, respectively.

It was shown[6,13] that, in the rigid (zeroth) approximation, a hierarchy of stable [minimum of mean AS interaction energy $\bar{v}$ per adatom in (B1)] configurations, so-called ideal epitaxial configurations [IEC's $(r_{x,y},\theta_{NW})$, (r_d,θ_{KS}), and a 2D (coherent) C], exists. This (i) provides energetic justification for the geometrical 1D and 2D matching criteria discussed in Sec. II and Appendix A, and (ii) shows that a specific IEC is related to specific Fourier coefficients A_i in (B1) and that its degree of stability and tendency to epitaxy (as measured by the depth $\Delta\bar{v}$ of its energy minimum) depends linearly on the A_i as follows:

$$\Delta\bar{v}=\begin{cases} WA, & \text{2D } C \text{ (pseudomorphic configuration)} \quad \text{(B5a)} \\ WA_1=WA_2, & \text{1D KS orientation} \quad \text{(B5b)} \\ WA_{3,4}, & \text{1D NW-}x\text{, NW-}y\ . \quad \text{(B5c)} \end{cases}$$

Here x or y specifies matching along the x or y direction in Fig. 1.

In the rigid model for (r,θ) values significantly different from the ideal ones[6,13] $\bar{v}(r,\theta)$ lie on a plateau $\bar{v}_0$. If the ML now assumes its elastic character, and (r,θ) can be imagined to approach ideality, oscillatory strains (MD's) at zero MS develop, positive strain energy ε is introduced, and $\bar{v}$ diminishes further until ultimately a limiting value $\bar{v}_1$ is reached, when a 1D or 2D coherent (ideal) configuration will be stable. If now the ML is appropriately misfit strained, (r,θ) assume the relevant ideal values, e.g., $(r_x,0)$ and $\bar{v}$ attains a minimum, $\bar{v}_2$ say, where $\bar{v}_0-\bar{v}_2=\Delta\bar{v}$ in (B1) and $\bar{v}_1-\bar{v}_2=\Delta\bar{v}/(1+P)$.[6,13] The stability of the coherent configuration requires that the energy change due to MS be negative or zero. Thus in the stability limit

$$\bar{\varepsilon}_e-\Delta\bar{v}/(1+P)=0\ , \quad \text{(B6)}$$

where $\bar{\varepsilon}_e$ is the mean MS energy per adatom. This equation may be solved in the form $l=l(r)$ or $r=r(l)$ for each of the IEC's in (B5), and presented pictorially in the form of phase boundaries $l(r)$ as in Fig. 4. The relations thus obtained,[12] using for $\bar{\varepsilon}_e$ the values

$$\bar{\varepsilon}_e=Wl^2(1-P^2)B_i(r-r_i)^2 \text{ for KS, NW-}x\text{, NW-}y\ ,$$
$$B_i=\frac{16R}{3(1-P^2)+2R(5-3P)}\equiv B,1,1\ , \quad \text{(B7a)}$$
$$r_i=r_d\approx 1..0887,\quad r_x\approx 0.9428,\quad r_y\approx 1.1547\ ,$$

and

$$\bar{\varepsilon}_e=2Wl^2(1+P)\left[[r-\tfrac{1}{2}(r_x+r_y)]^2+\frac{(1-P)(r_y-r_x)^2}{4(1+P)}\right] \text{ for 2D } C\ , \quad \text{(B7b)}$$

are

$$r(l)=r_i\pm\frac{1}{l}\left[\frac{A_iB_i}{(1-P)(1+P)^2}\right]^{1/2} \text{ for KS, NW-}x\text{, NW-}y\ , \quad \text{(B8a)}$$

$$A_i=A_1=A_2,A_3,A_4\ ,$$

and

$$r(l)=\tfrac{1}{2}(r_x+r_y)\pm\left[\frac{A}{2(1+P)^2l^2}-\frac{(1-P)(r_y-r_x)^2}{4(1+P)}\right]^{1/2} \text{ for 2D } C\ . \quad \text{(B8b)}$$

In order to construct a properly interconnected stability limit (phase diagram), the relations (B8) must be supplemented by additional ones (not published previously) to define the transition from one IEC (coherent region) to an adjacent one. The desired relations are provided by the lines of intersection of the corresponding energy surfaces, the energy reference being the rigid configuration with parameters (r,θ,l) well away from ideal values. For example, the 1D NW-x and 2D C energy surfaces intersect when

$$(\bar{\varepsilon}-\Delta\bar{v})_{1D\ NW\text{-}x}-(\bar{\varepsilon}-\Delta\bar{v})_{2D\ C}=0\ . \quad \text{(B9)}$$

Where more than two surfaces are present, the appropriate lines of intersection are selected by using minimum-energy considerations. Thus one finds that three small though significant regions of interest exist in Fig. 4: two narrow channels neighboring *DE* and *FG* and a displaced transition boundary *HI*. In the channel 1D NW-x and 2D C, 2D C has the lower energy, but is itself unstable with respect to the introduction of a parallel array of MD's (compare also curves A in Fig. 3). This generates a NW-x configuration which differs from the 1D NW-x configuration only in that the component of strain normal to the coherent one is oscillatory (MD's) rather than homogeneous. The equations for the boundaries *DE*, *FG*, and *HI*, thus obtained from (B7) and (B9) are, respectively,

$$l(r)\begin{cases} \dfrac{1-A_3}{|r(1+P)-r_y-Pr_x|} & \text{for 2D } C\text{/NW-}x \text{ boundary,} \quad \text{(B10a)} \\ \left\{\dfrac{(1-P^2)(B^2-1)}{A_1-A_4}\left[\left[r-\dfrac{Br_d-r_y}{B^2-1}\right]^2-\dfrac{B^2(r_d-r_y)^2}{B^2-1}\right]\right\}^{-1/2} & \text{for 1D KS/1D NW-}y \text{ boundary,} \quad \text{(B10b)} \\ \left[\dfrac{(1+P)Q}{1-A_1}[(r-D)^2-E]\right]^{-1/2} & \text{for 2D } C\text{/1D KS boundary ,} \quad \text{(B10c)} \end{cases}$$

$$Q=2-B(1-P),\quad D=[r_x+r_y-B(1-P)r_d]/Q\ ,$$

$$E=(1-P)[B(1+P)(r_x+r_y-2r_d)^2-Q(r_x-r_y)^2]/2Q^2(1+P)\ .$$

An exact analysis, allowing for oscillatory strains, does not exist. An approximate analysis[13,14] has been carried out though, assuming oscillatory strains (MD's) in one direction and homogeneous strains (MS's) in the perpendicular direction; the so-called *striped* configuration. Mathematical tractability needed additional simplifying approximations:[13,14] the replacement of differences in the equilibrium and other relations, by differentials, and in some cases, a limitation on the elastic (stiffness) constants. In all cases the equilibrium equations reduce to Sine-Gordon-type equations whose solutions describe the accommodation of misfit between monolayer and substrate in terms of MD's, MS's, and a misfit vernier (MV); the latter, which is exact for the rigid model, is a limiting form of a superposition of the previous two, when the stiffness and/or misfit becomes large.

The analysis[13,14] yields, for comparable cases, essentially the same results for the stability limits in Eq. (B8a). Only the "square root expressions" differ by a factor

$$\left[\left[\frac{A_iB_i}{(1-P)(1+P)^2}\right]^{1/2}\right]_{\rm hom}\Bigg/\left[\left[\frac{A_iB_i}{(1-p)(1+P)^2}\right]^{1/2}\right]_{\rm osc}=\frac{\pi}{2}\left[\frac{1-P}{2}\right]^{1/2}, \tag{B11}$$

close to unity; about 0.9 for realistic values of P. In order that this be true for the KS case, the value of R in B of Eq. (B7) was limited to $R=\frac{1}{2}(1-P)$ (isotropic elasticity), as was needed for the analysis with oscillating strains.[14(c)] A complete equivalent of the 2D C homogeneous case has not been dealt with. The closest is the breakdown of the 2D C case via so-called complete misfit dislocations[14(a)] at

$$r=\tfrac{1}{2}(r_x+r_y)+\frac{(1-P)(r_x-r_y)}{2(1+P)}-\frac{1}{l}(2A_1)^{1/2}\frac{\Gamma_x}{\pi(1+P)} \tag{B12}$$

for small r with $\Gamma_x\simeq 3.0900$. The corresponding relation for large r is obtained by interchanging x and y, replacing the minus sign at the last term with a plus sign, and using $\Gamma_y\simeq 3.0070$. Note that intermediate values of r are not covered by these relations.

The following relations compounded from Ref. 14(a) have been used in constructing Fig. 5 in order to illustrate the modification of the *ML* atomic arrangements induced by the coexistence of MD's and MS's; the NW-x orientation is used as an example:

$$\bar{l}=\frac{r_x l\kappa F[\kappa,\pi(\bar{u}-\frac{1}{2})]}{\pi(2A_1)^{1/2}}\ , \tag{B13a}$$

$$\bar{P}=\frac{2^{1/2}r_x lK(\kappa)}{\pi(A_1)^{1/2}},\quad \bar{e}_y=-P[r_x r^{-1}(\bar{P}^{-1}+1)-1]\ , \tag{B13b}$$

$$r=r_x-\frac{(2A_1)^{1/2}}{l\kappa(1-P^2)}\left[\frac{2E(\kappa)}{\pi}+\frac{\pi P^2}{2K(\kappa)}\right]. \tag{B13c}$$

Here F and K are incomplete and complete elliptic integrals of the first kind with modulus κ, E is the complete elliptic integral of the second kind, $\bar{l}$ enumerates atomic rows perpendicularly aligned to the x axis (Fig. 1), $\bar{u}(\bar{l})$ is the displacement of row $\bar{l}$ in units of row spacing; $\bar{P}$ is the MD spacing and $\bar{e}_y$ the homogeneous (Poisson) strain in the y direction due to MS $\bar{e}_x$ in the x direction. Equation (B13c) determines, for given $r<r_x$, the modulus κ which has been used as a convenient parameter.

APPENDIX C: GROWTH MODE, SUPERSATURATION, AND MOBILITY

In the original derivation[21] the condition for monolayer-by-monolayer growth (FM growth) was found to be $\Delta\gamma_n=\gamma_f+\gamma_{in}-\gamma_s\leqq 0$. In present day language this means each layer has to wet the preceding one. As long as this condition is fulfilled the film can grow even at undersaturation ($\Delta\mu<0$), but as soon as it is violated three-dimensional nucleation is necessary for condensation which is only possible under supersaturation conditions ($\Delta\mu>0$). The size and shape of the critical nucleus is determined by the extrema of the free enthalpy $G(N,\xi_i)$ as a function of the number N of the atoms in the nucleus and of the parameters ξ_i characterizing its shape, i.e., by $(\partial G/\partial N)_{\xi_i}=0$ and $(\partial G/\partial\xi_i)_N=0$ for the size and shape, respectively. For the simplest example of a prism of height h with square base of side length 1 and the specific free-surface energies γ of the top and the four side faces, we obtain $\xi=h/1=\Delta\gamma/(2\gamma)$ and $N=32v_0^2\gamma^2\Delta\gamma/(\Delta\mu)^3$. Here $\Delta\gamma=\gamma+\gamma_i-\gamma_s$ and v_0 is the atomic volume. The side length and height are given by $1=4v_0\gamma/\Delta\mu$ and $h=2v_0\Delta\gamma/\Delta\mu$, respectively.

The first reasoning leading to a supersaturation-induced FM growth is based on the dependence of h on $\Delta\mu$. This mode should occur when $\Delta\mu$ exceeds the critical value $\Delta\mu_c$ at which h is the height of one monolayer.[26,55] If each atom is assigned a cube of edge length b, then this condition may be written as $\Delta\mu_c=2b^2\Delta\gamma$. The fallacy of this reasoning becomes clear when 1 and N for $\Delta\mu=\Delta\mu_c$ are considered: $1_c=h_c/\xi=2b\gamma/\Delta\gamma$, $N_c=4(\gamma/\Delta\gamma)^2$. For $\gamma=2\gamma_s$ and $\gamma_i=0$, $1_c=2h_c$ and $N_c=4$. Unless surface mobility is so limited that small particles cannot approach their equilibrium shape, the particles will grow laterally

and outward and will be several monolayers thick at the time at which they merge laterally into a continuous layer. Only with extremely high nucleation rates and negligible mobility—to avoid post-nucleation clustering into the equilibrium shape—could a monolayer be formed, but this is incompatible with the assumptions—shape and size determined by thermodynamics—on which the $\Delta\mu_c$ criterion is based.

The second derivation of the supersaturation-induced FM growth criterion[26] starts from a comparison of three- and two-dimensional crystals consisting of the same number N of atoms. The free enthalphy change in the formation of the critical nucleus is different in the two cases. For sufficiently small N, $\Delta G_2 < \Delta G_3$ so that two-dimensional nuclei are formed provided $\Delta\mu$ is sufficiently high. The critical supersaturation at which this occurs is again $\Delta\mu_c = cb^2\Delta\gamma$, where $c=2$ and $\sqrt{3}$ for fcc (100) and (111) oriented crystals, respectively.[26] The reason why $\Delta G_2 < \Delta G_3$ for sufficiently small N is an energetic-geometrical reason and can be seen easily in a simple bond-breaking example. Consider an fcc (100) surface and an fcc (100) layer with $b=a$ and only first-nearest-neighbor interactions between film atoms ($\psi_{ff}=\psi$) and between film and substrate atoms ($\psi_{fs}=\psi'$). A "three-dimensional" nucleus consisting of four atoms in the first layer and one atom in the center in the second layer has the total bonding energy $16\psi' + 8\psi$, the two-dimensional nucleus $20\psi' + 5\psi$. Thus if $\psi' > (3/4)\psi$, a two-dimensional cluster consisting of five atoms is more stable than a three-dimensional one. If $\psi' > (4/5)\psi$, this is true for even larger clusters, e.g., $N=16$. It appears, therefore, that when ψ' is not much smaller than ψ, monolayer growth may occur at sufficiently high supersaturation.

This is, however, an erroneous conclusion because the same criterion which favored the two-dimensional cluster at small N values—maximum binding energy—leads with increasing particle size to a conversion from two-dimensional to three-dimensional particles. Detailed bond-breaking calculations as a function of N show that this 2D–3D transition occurs at small N unless ψ' is close to ψ which is equivalent to $\Delta\gamma \approx 0$. Only if kinetic limitations hinder the attainment of the optimum particle configuration can the quasi-two-dimensional configuration be frozen in. Thus, this reasoning for a supersaturation-induced FM growth condition $\Delta\mu_c = cb^2\Delta\gamma$ is also without a sound foundation.

With the theoretical arguments discounted the experimental evidence for this growth mechanism and the condition $\Delta\mu_c = cb^2\Delta\gamma$ still has to be examined. Most of the various experimental studies quoted as support of the theoretical predictions[26,55] only show that at low temperatures, e.g., room temperature, the film is already continuous at a few monolayers thickness which is also expected for three-dimensional nuclei because of the high nucleation rate and low mobility. Only one study[56] seems to confirm the relation $\Delta\mu_c = cb^2\Delta\gamma$ by a detailed investigation of the growth of Fe on Cu (111) with Auger electron spectroscopy and low-energy electron diffraction. A critical examination of the data indicates, however, that monolayer growth does not occur and that the $\Delta\mu_c$ versus $\Delta\gamma$ relation is not fulfilled. Evidence against the monolayer growth analysis is the large inelastic mean free path of the Fe and Cu Auger electrons—9.2 Å, after taking the instrument correction factor 1/0.74 into account—which is twice as large as the accepted values and indicates non-monolayer growth. Evidence against the theoretical $\Delta\mu_c$ versus $\Delta\gamma$ relation is the high $\Delta\gamma$ value—3.46 Jm^{-2}—deduced from the experiment. This is three times larger than expected. The explanation given, a strong temperature dependence of γ_{Fe} and γ_{Cu}, is not acceptable because it would require unphysically large surface entropies.[28] Thus there is no experimental evidence for the thermodynamically derived supersaturation-induced FM growth.

Therefore, the cause for the observed quasi-FM growth has to be sought in the kinetics of the deposition process. When thermodynamics favors three-dimensional particles monolayerlike growth can be approached by eliminating atomic mobility so that the equilibrium shape cannot form. Some information on the resulting growth mode can be deduced from Monte Carlo simulations in which complete absence of surface diffusion, simple cubic lattices with identical lattice constants for film and substrate, and site-dependent effective sticking coefficients (attachment minus detachment probability), were assumed.[57] In the experimental situation in which quasi-FM growth is observed the sticking coefficient is site-dependent equal to one and there is still some mobility. This corresponds approximately to the high supersaturation limit of the Monte Carlo calculations, for the growth of A on A, which yield a mean film thickness at 99% substrate coverage of about 4.5 monolayers and an interface width—defined by 99% occupation in first and 1% occupation in topmost layer—of about 10 monolayers.

The kinetics problem was also addressed analytically by Kashchiev *et al.*[58] He clearly recognized that the thermodynamic criterion of a monolayer thick nucleus is not sufficient to decide the growth mode but that this is rather determined by the kinetics of the subsequent growth. He described the growth by Avrami's theory of crystallization which—as already noted previously[59]—leads to usable analytical expressions only when serious simplifications are made. For example, the assumption of constant nucleation rate and constant lateral growth velocity which is extensively discussed in Ref. 58 (case $m_i=3$) is incompatible with constant deposition rate. Only the case $m_i=1$ in Ref. 58 for growth on its own substrate simulates the experiment to a certain extent. In this case a mean thickness for 99% coverage of 4.61 monolayers and an interface width of 8.2 monolayers is obtained in good agreement with the Monte Carlo simulations. Thus, the kinetic considerations show that in the absence of surface diffusion no quasi-FM growth occurs. A certain amount of mobility must be present to smooth out the statistical thickness fluctuations, but it may not be so high as to allow the particles to achieve their equilibrium shape characterized by $\xi = h/1$, unless $\xi \ll 1$.

The conclusions from this appendix are as follows: (1) The generalization of the thermodynamic condition $\Delta\gamma \leqq 0$ to $\Delta\gamma \leqq \Delta\mu/cb^2$ in the case where $\Delta\gamma > 0$ is not a valid criterion for FM growth. (2) In the case $\Delta\gamma > 0$ quasi-Fm growth can be achieved under kinetic conditions which give a high nucleation rate and limited mobility.

*Permanent address: Physikalisches Institut der Technischen Universität Clausthal, D-3392 Clausthal-Zellerfeld, Federal Republic of Germany.

[1]C. M. Falco and I. K. Schuller, in *Synthetic Modulated Structures/VLSI,* edited by L. L. Chang and B. C. Giessen (Academic, Orlando, 1985).

[2]C. S. L. Chun, G.-G. Zheng, T. L. Vincent, and I. K. Schuller, Phys. Rev. B **29**, 4915 (1984), and references therein.

[3]E. Bauer, in *The Chemical Physics of Solid Surface and Heterogeneous Catalysis,* edited by D. A. King and D. P. Woodruff (Elsevier, Amsterdam 1984), Vol. III B, p. 1.

[4]R. Ramirez, A. Rahman, and Ivan K. Schuller, Phys. Rev. B **30**, 6208 (1984).

[5]L. A. Bruce and H. Jaeger, Philos. Mag. A **38**, 223 (1978).

[6]Jan H. van der Merwe, Philos. Mag. A **45**, 145 (1982).

[7]L. C. A. Stoop, Thin Solid Films **42**, 33 (1977).

[8]L. C. A. Stoop, Thin Solid Films **62**, 115 (1979).

[9]L. C. A. Stoop, Thin Solid Films **103**, 375 (1983).

[10]T. Halicioglu, H. O. Pamuk, and Ş. Erkoç, Surf. Sci. **143**, 601 (1984).

[11]Brian W. Dodson, Phys. Rev. B **30**, 3545 (1984).

[12]Jan H. van der Merwe, Philos. Mag. A **45**, 159 (1982).

[13]J. H. van der Merwe, Thin Solid Films **74**, 129 (1980).

[14](a) L. C. A. Stoop and J. H. van der Merwe, Thin Solid Films **91**, 257 (1982); (b) **94**, 341 (1982); (c) **98**, 65 (1982).

[15]L. C. A. Stoop, Thin Solid Films **94**, 353 (1982).

[16]M. Braun and J. H. van der Merwe (unpublished).

[17]F. Auret and J. H. van der Merwe, Thin Solid Films **23**, 257 (1974).

[18]I. Markov and A. Milchev, Surf. Sci. **136**, 519 (1984); **145**, 313 (1984).

[19]F. C. Frank and J. H. van der Merwe, Proc. R. Soc. London, Ser. A **198**, 205 (1949); **198**, 216 (1949); **200**, 125 (1949).

[20]C. A. B. Ball, Phys. Status Solidi **42**, 357 (1970).

[21]E. Bauer, Z. Kristallogr. **110**, 372 (1958).

[22]J. G. Dash, Phys. Rev. B **15**, 3136 (1977); J. Phys. (Paris) Colloq. **38**, C4-201 (1977).

[23]R. Pandit, M. Schick, and M. Wortis, Phys. Rev. B **26**, 5112 (1982).

[24]C. Ebner, C. Rottman, and M. Wortis, Phys. Rev. B **28**, 4186 (1983).

[25]S. J. Kennedy and J. S. Walker, Phys. Rev. B **30**, 1498 (1984).

[26]I. Markov and R. Kaischew, Krist. Tech. **11**, 685 (1976); Thin Solid Films **32**, 163 (1976).

[27]D. Kashchiev, J. Cryst. Growth **40**, 29 (1977).

[28]L. Z. Mezey and J. Giber, Jpn. J. Appl. Phys. **21**, 1569 (1982).

[29]E. Bauer, Appl. Surf. Sci. **11/12**, 479 (1982).

[30]J. H. van der Merwe, in *Chemistry and Physics of Solid Surfaces V,* edited by R. Vanselow and R. Howe (Springer-Verlag, Berlin, 1984), p. 365.

[31]Unpublished data of the collaborators of one of the authors (E.B.).

[32]M. Sagurton, M. Strongin, F. Jona, and J. Colbert, Phys. Rev. B **28**, 4075 (1983), and references therein.

[33]J. Kołaczkiewicz and E. Bauer, Surf. Sci. **144**, 495 (1984).

[34]Ch. Park, E. Bauer, and H. Poppa, Surf. Sci. **154**, 371 (1985).

[35]E. Bauer and H. Poppa, Thin Solid Films **12**, 159 (1984).

[36]A. Pavolvska, M. Paunov, and E. Bauer, Thin Solid Films **126**, 129 (1985).

[37]J. A. A. Engelbrecht and H. C. Snyman, Thin Solid Films **59**, 345 (1979); **66** L1 (1980); **69**, 301 (1980), and references therein.

[38]G. Honjo, K. Takayanagi, K. Kobayashi, and K. Yagi, J. Cryst. Growth **42**, 98 (1977).

[39]H. C. Snyman and G. H. Olsen, J. Appl. Phys. **44**, 889 (1973); Acta Metall. **21**, 769 (1973).

[40]J. Kołaczkiewicz and E. Bauer (unpublished).

[41]A. D. Novaco and J. P. McTague, Phys. Rev. Lett. **38**, 1286 (1977); J. Phys. (Paris) Colloq. **38**, C4-116 (1977).

[42]J. P. McTague and A. D. Novaco, Phys. Rev. B **19**, 5299 (1979).

[43]H. Shiba, J. Phys. Soc. Jpn. **46**, 1852 (1979); **48**, 211 (1980).

[44]C. R. Fuselier, J. C. Raich, and N. S. Gillis, Surf. Sci. **92**, 667 (1980).

[45]References to the original work can be found in the compilation by J. P. Biberian and G. A. Somorjai, J. Vac. Sci. Technol. **16**, 2073 (1979).

[46]K. Takayanagi, Surf. Sci. **104**, 527 (1981), and references therein.

[47]Ch. Park, E. Bauer, and H. Poppa (unpublished).

[48]K. Christmann, G. Ertl, and H. Shimizu, Thin Solid Films **57**, 247 (1979); J. Catal. **61**, 397 (1980).

[49]S. Calisti, J. Suzanne, and J. A. Venables, Surf. Sci. **115**, 455 (1982).

[50]C. G. Shaw, S. C. Fain, Jr., and M. D. Chinn, Phys. Rev. Lett. **41**, 955 (1978).

[51]D. L. Doering and S. Semancik, Phys. Rev. Lett. **53**, 66 (1984).

[52]E. Bauer, H. Poppa, and G. Todd, Thin Solid Films **28**, 19 (1975).

[53]Ch. Park, H. M. Kramer, and E. Bauer, Surf. Sci. **119**, 251 (1982).

[54]W. A. Steele, Surf. Sci. **36**, 317 (1973).

[55]R. Kaischew, S. Stoyanov, and D. Kaschiev, J. Cryst. Growth **52**, 3 (1981).

[56]U. Gradmann, W. Kümmerle, and P. Tillmanns, Thin Solid Films **34**, 249 (1976); Phys. Status Solidi A **44**, 539 (1977).

[57]D. Kashchiev, J. P. van der Eerden, and C. van Leeuwen, J. Cryst. Growth **40**, 47 (1977).

[58]D. Kashchiev, J. Cryst. Growth **40**, 29 (1977).

[59]E. Bauer, A. K. Green, K. M. Kunz, and H. Poppa, *Basic Problems in Thin Film Physics,* edited by H. Mayer and R. Niedermayer (Vandenhoeck and Ruprecht, Göttingen, 1966), p. 135.

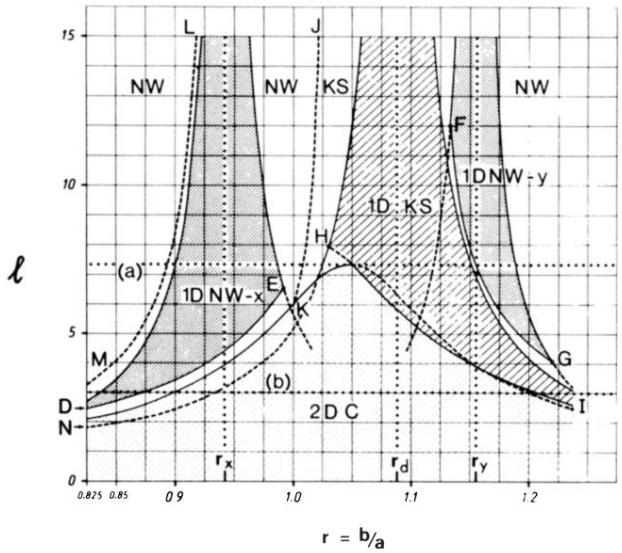

FIG. 4. Stability ranges ("phases") in (r,l) variables for pseudomorphy (2D C), 1D coherency in NW orientation (1D NW-x, NW-y) and 1D coherency in KS orientation (1D KS) of homogeneously strained (111) fcc monolayers on (110) bcc substrates with $P=0.419$ and $R=0.939$ as in Fig. 3. The dotted lines (a) and (b) represent, respectively, the cases depicted in Figs. 3(a) and 3(b). In the corridor DE, 2D C has the lower energy but is itself unstable and misfit dislocation (MD) formation (associated with curves A in Fig. 3) transforms it into a NW orientation. In the corridor FG, KS is more stable but the orientation less certain.